APPLICATION OF AVIRIS WATER MAPPING CAPABILITIES TO THE PROBLEM OF REGIONAL SURFACE EVAPORATION

James E. Conel, Veronique Carrere, Robert O. Green, Jack S. Margolis, Carol Bruegge, Ronald E. Alley, Gordon Hoover, and Anne Nolin

Jet Propulsion Laboratory
California Institute of Technology
Pasadena, California

Introduction

Water vapor plays a major role in the energetics of the Earth's atmosphere. Despite its importance quantitative knowledge of global and even regional water and energy budgets is still lacking (WMO/TD No. 215). In hydrological work there is still no agreement on how regional evaporation at the river basin scale should be measured (Brutsaert, 1986). Well-established methods exist for point measurements using micrometeorological data (e.g., eddy correlation, energy budget and mean profile) (Brutsaert, 1982) and it would be straightforward to make large areal estimates from networks of such stations if such data sets were routinely available.

The focus of the present study is exploration of how the rapid, high-spatial-resolution, atmospheric water mapping capabilities of AVIRIS can be utilized, perhaps involving time sequences of observations, to provide a link between point measurements and larger areal or regional estimates of surface evaporation.

Atmospheric Water Vapor Measurements Provided by AVIRIS

AVIRIS makes measurements of the upward-directed spectral radiance between 400 and 2450 nm at an observational altitude of 20 km above the Earth's surface. The spectral resolution of about 10 nm allows resolution of the important near infrared atmospheric absorptions related to water vapor, among them are the bands at 940 and 1130 nm. We reported (Conel *et al.*, 1988; Conel *et al.*, 1989) the use of a simple two band ratio algorithm and the atmospheric model LOWTRAN 6 to derive estimates of the column abundance of atmospheric moisture. Subsequent modification of this algorithm using LOWTRAN 7 (*e.g.*, the so-called continuum interpolated band ratio (CIBR) of Green *et al.*, 1990) was introduced to account for multiple scattering and to help compensate for vulnerability of the initial simple ratio algorithm to surface reflectance variations because of surface vegetation or soil moisture. Frouin and Middleton (1990) presented another ratio algorithm based on the Tanre 5S code involving use of a narrow and a wide spectral channel centered on one another at the maximum of absorption of the 940 nm water band, and also designed to minimize surface reflectance interference. These ratio methods require assumptions about the atmospheric scattering model and the visibility or measurement of these critical parameters. These methods are subject to systematic errors in retrieved abundances with departures from the assumptions (Carrere *et al.*, 1990; Carrere and Conel, 1991). Gao and Goetz (1990) employed a nonlinear least square band fitting technique with the water absorption band model of Malkmus to provide estimates of atmospheric and surface moisture components. Their method does

not account for atmospheric scattering and is therefore best applied under conditions of high visibility (> 50 km). Green *et al.* (1991, these proceedings) developed a least square band fitting technique based on the MODTRAN atmospheric radiative transfer code that simultaneously estimates parameters of a surface reflectance model together with atmospheric moisture. The method specifically accounts for atmospheric water vapor absorption and aerosol multiple scattering through the MODTRAN model, once visibility is constrained in the code. The technique accounts for the presence of surface water resident in vegetation, as soil moisture, and as standing water, and appears capable of atmospheric moisture retrievals over water by using the path radiance term and the in-band combined absorption and scattering treatment contained in the model. The separation of surface and atmospheric moisture is possible because of differences in band shape and position (surface water shifted to "red") among these components.

We have compared the water abundances retrieved from AVIRIS via the LOWTRAN 7 code with column abundances measured simultaneously on the ground with a sun photometer (Bruegge *et al.*, 1990; Carrere and Conel, 1991) with agreement to within a few percent. Independent confirmation of these measurements was provided by comparison with column abundance retrievals from single-line atmospheric water vapor observations made with a high resolution Fourier Transform spectrometer (Bruegge, *et al.*, 1990). These latter estimates are derived from band parameters and a multiple-layer atmospheric line-by-line transmission model. The LOWTRAN 7-based and interferometer-based estimates agree to within 3%, whereas the scatter of the interferometer determinations using multiple lines was about 5%.

The precision of the described atmospheric water vapor retrievals has been estimated based on the noise characteristics of AVIRIS for the CIBR and Frouin algorithms using radiance measurements over water bodies where the surface reflectance is near zero. For example, for October 1990 observations at Salton Sea (Carrere and Conel, 1991), the uncertainties in water recoveries are less than about 10% for the CIBR, and less than about 2% for the Frouin algorithm, including both random and coherent noise components. The Frouin algorithm enjoys this advantage from use of multiple radiance measurements across the band in the algorithm.

The whisk-broom scanning mode of AVIRIS samples the ~11-km cross-track swath in increments of about 20 m, each in 1/12 of a second, or 100 km^2 in 42 sec. The total horizontal length of lines sampled per 100 km^2, considered as a profile, is nearly 5600 km. The time between possible successive AVIRIS observations over the same target may be constrained by operational considerations of the ER-2 aircraft platform at 11-12 minutes.

Application to the Problem of Regional Surface Evaporation

We investigated three well-known methods of estimating land (or water) surface evaporation: (1) a bulk transfer formulation (*e.g.*, Brutsaert, 1982; Liu, 1990), (2) the atmospheric water budget with surface evaporation evaluated as a residual (*e.g.*, Brutsaert, 1982), and (3) a water budget method employed regionally with long time averages (e.g., Peixoto, 1973; Peixoto and Oort, 1983). How can observations provided by AVIRIS, namely column moisture abundance and its changes with time from place to place, be used in applications of these methods?

(1) Bulk Transfer

A typical procedure for watershed-scale surface (Brutsaert, 1982, 1986) and ocean evaporative flux measurement (Liu, 1990) is based on application of the equation

$$E = C_E U_r \rho (q_s^*(T_s) - q_r) \qquad (1)$$

where E is the surface evaporation in g/(cm^2 sec), C_E is the bulk transfer coefficient for water vapor, U_r the mean horizontal wind speed at reference height z_r above the surface, ρ the atmospheric density, $q_s^*(T_s)$ the saturation specific humidity at the surface temperature T_s, and q_r the mean specific humidity at the reference height. AVIRIS observations of water column abundance distribution in and of themselves cannot supply the surface temperature nor estimates of C_E, which must be obtained independently from in situ measurements or theoretical analysis (Deardorff, 1968; Liu *et al*, 1979; Brutsaert, 1979). The need to estimate C_E together with a surface resistance (in lieu of the term $q_s^*(T_s)$ in Equation 1 has led Brutsaert and Mawdsley (1976) to consider use of a uniform boundary layer model based on similarity principles for estimation of E. This model requires use of radiosonde data to obtain values of wind, temperature, and humidity at the upper and lower surfaces of the boundary layer.

Empirical relationships between the column abundance W supplied by AVIRIS and the specific humidity near the surface q_r may, however, be useful in estimating the latter quantity. Following Liu (1990) and others [see references in Liu (1990)] we compiled data from 2105 Rawinsonde flights (1986 to present) from Edwards Air Force Base, California (a desert environment), correlating total column water vapor abundance observed versus the ground-level absolute humidity. The resulting scatter plot, not edited for possible faulty observations, is shown in Figure 1. The trends illustrated are similar to those in radiosonde data compiled by Liu (1986) for oceanic sites, but with greater scatter in the present instance.

The preliminary compilation of Figure 1 is being extended to other Rawinsonde data sets including oceanic and coastal sites. The analysis of such might profitably be extended to seek additional (empirical) correlations of boundary layer thickness with absolute humidity at the upper boundary. Another area of interest is compilation of sun photometer measurements of water column abundance with measurements of ground-level absolute humidity that are independent of the Rawinsonde column measurement process. Such spectroscopic-based correlations will represent instantaneous line-of-sight to the sun measurements as opposed to ~1-hour-long averages characteristic of balloon ascents and will serve to characterize the time scale of surface humidity-column abundance correlations such as those depicted in Figure 1.

(2) Atmospheric Water Budget

Basis of the method – This method (see Peixoto, 1973; Brutsaert, 1982, p. 257ff.) evaluates the surface evaporation as a residual of the terms of the water budget equation for a control volume in the atmosphere. The general water balance equation for the atmosphere at a point is

$$\frac{\partial W}{\partial t} + \nabla \cdot \int_0^\infty U(z) q \rho dz = E - P \qquad (2)$$

where W is the column abundance, equal to $\int_0^\infty q\rho dz$, and U(z) is the horizontal wind velocity vector. The z-axis is vertical, positive upward, and t is the time. The right hand side of Equation 2 is the difference between evaporation and precipitation at the point considered. Multiplication by dA/A and integration over the horizontal extent of the volume secures the required areal average. Where areal averages are derived below from image data, they will be denoted by overbars. To simplify the discussion, we consider a situation of uniform unidirectional winds with height over the control volume so that rotation of the horizontal coordinate axes about the vertical reduces the divergence operator to a single derivative $\partial/\partial s$, say, where the s-axis is positive in the direction of the wind, whose velocity is $U_s(z)$. The integral in Equation 2 must be transformed to quantities observable by AVIRIS. This can be accomplished using the first theorem of mean value (Carslaw, 1950, p. 105ff.), in which case the integral becomes

$$\bar{U}_s \int_{z_0}^{z_t} q\rho dz = \bar{U}_s W \qquad (3)$$

In equation 3 z_0 is the surface height and z_t is the height of the top of the internal water vapor boundary layer. If $U_s(z)$ is continuous, U_s is given by

$$\bar{U}_s = \left[1/(z_t - z_0)\right] \int_{z_0}^{z_t} U_s(z) dz \qquad (4)$$

With these definitions, Equation 1 is transformed to

$$\frac{\partial W}{\partial t} + \bar{U}_s \frac{\partial W}{\partial s} = E - P \qquad (5)$$

All of the quantities on the left hand side of Equation 5 are, in principle, derivable from the AVIRIS images of W over a given area, the time derivative from sequences of images, and the spatial derivative point by point for each image from finite difference approximations. The spatial scale of recoverable fluctuations is $\geq$ 20 m for W and 40 m for $\partial W/\partial s$. The importance of variations below these lengths will need to be evaluated with field observations in particular cases.

Interpretation of the velocity $\bar{U}_s$ – The interpretation of $\bar{U}_s$ is more problematical. In this preliminary analysis we sought guidance from studies of the influence of wind shear on horizontal dispersion for instantaneous ground-level sources (Saffman, 1962; Smith, 1965; Csanady, 1969; Taylor, 1982). If the moisture is confined within a layer of constant thickness and there is neither loss nor gain of material at the upper and lower boundaries, then $\bar{U}_s$ can be thought of as the speed of horizontal translation of centroids of spatial fluctuations in W seen in successive images. If the atmosphere is unbounded, and the wind speed U(z) and eddy diffusivity K(z) increase upward according to az^m and bz^m respectively, then according to results of Saffman (1962) the centroid for a ground-level release at time t = 0 advances proportional to $at(bt)^{m/(2-n)}$. If the wind speed increases linearly with height (m = 1) and K is constant,

the centroid displacement is $\propto t^{3/2}$ (Saffman, 1962; Smith, 1965), and the speed $\propto t^{1/2}$. For power law variations in U and K with z, adopting values of m = 1/7 and n = 6/7 (*e.g.*, Brutsaert, 1982) gives a centroid translation $\propto t^{9/8}$ and speed $\propto t^{1/8}$. For all of these unbounded models, the apparent translation speed increases with time as material originally at the surface diffuses to regions of greater and greater wind speed at altitude.

In addition to wind shear in the surface layer, the trajectories of particles are influenced both by Coriolis forces and surface drag in the Ekman layer. Diffusion in the Ekman layer has been analyzed by Csanady (1969) and more recently by Taylor (1982). Figure 2 is taken from the latter paper. Initially symmetric instantaneous releases at the surface are quickly distorted into ellipsoidal-shaped distributions by wind shear. As time passes, the concentration distributions, here depicted by ellipses representing isopleths at a given height where the concentration is 60% of the centroid value, are displaced in the direction of ground-level wind shear. These distributions elongate, broaden, and twist in response to lateral diffusion and the change of wind direction aloft, with axes connecting centroids between levels eventually aligned with one another and at 45° to the geostrophic wind. Since a continuous surface source, say from evaporation of a small water body or wet field, might be visualized as a continuous distribution of such releases, an expanding rotated plume could be expected to emerge wherever atmospheric conditions permit Ekman spiral structures to form in the atmosphere.

AVIRIS water vapor image sequences and Rawinsonde data at Rogers Dry Lake-To investigate the question of recovering atmospheric motions from the water vapor maps, we used a sequence of four images obtained at Rogers Dry Lake, California as shown in Figure 3 (see paper by Green *et al.*, 1991 in these proceedings for color slides of these images). These data were acquired on July 23, 1990 as part of the in-flight radiometric calibration and stability analysis of AVIRIS. The water vapor column abundance maps were generated using the CIBR algorithm, and the data were filtered over 7 × 7 pixel subareas. The lower images depict the clear air conditions over the site as seen at a wavelength of 892 nm.

A rawinsonde was launched from Edwards Air Force Base at 1829 hr UCT and provided data on winds, temperature, and moisture aloft during a portion of the first AVIRIS overpass. The approximate trajectory of the balloon ascent from its point of origin is superposed on the first image panel (Fig. 3). The lower part of the ascent trajectory exhibits a clockwise rotation from ground level to approximately 6000 feet, possibly describing motion in the Ekman wind spiral. The winds aloft, absolute humidity and the total precipitable water distributions obtained are given in Figure 4.

Estimating $\bar{U}_s$ from image data – Two methods were used to derive estimates of $\bar{U}_s$ from the AVIRIS water map sequence at Rogers Dry Lake: (tracking of water cloud features between successive images, and (2) calculation of $\bar{U}_s$ from Equation (5).

Method 1 - Estimation of the average wind velocity from displacements of recognizable features in the column abundance distribution between successive images is straightforward to apply in principle, but difficult in practice because of large rapid changes in the distributions of W between

successive AVIRIS frames arising from shear, rotation, and diffusion. We studied the image sequence of Figure 3 for features and patterns that could be identified from image to image. While several candidate pairs could be identified, none were straightforward to match; furthermore it proved difficult to avoid a prejudice of wind direction (and to a lesser extent speed) induced by the rawinsonde results for that time period. Simple vectorial diagrams of the displacements for a few examples are shown in Figure 5. The evolution of such water vapor features would be aided by AVIRIS water images more closely spaced in time than the 11-12 minute intervals achieved in making the observations presented in Figure 3.

It is worth pointing out that the feature tracking method described here yields, according to Equation 5, a value for the average velocity $\bar{U}_s$ that will be independent of the presence of source or sink terms provided that these terms are constant in space but not necessarily in time. For example, the solution of Equation 5 for the initial value $W(x,0) = f(x)$ and a source term $\epsilon(x,t)$ is $W(x,t) = f(x - \bar{U}_s t) + \int_0^t \epsilon(\bar{U}_s \xi + x - \bar{U}_s t, \xi) d\xi$ (Zauderer, 1989). The initial pattern f(x), which can be introduced by advection, translates along the + x-axis with velocity $\bar{U}_s$, but is modified by the second term, if $\epsilon = \epsilon_0 g(t)$, $W(x,t) = f(x - \bar{U}_s t) + \epsilon_0 \int_0^t g(\xi) d\xi$, and the pattern translates along the + x-axis with velocity $\bar{U}_s$.

The tracking of features in the column abundance advancing under advection is feasible and can be seen from examination of Figure 6. These ground based data were acquired with water vapor channels of Reagan solar photometers at Ivanpah Playa in eastern California on March 7, 1991. The instruments were separated by approximately 1500 m along a line trending N30°W. The hourly average wind speed, wind direction, and standard deviation of the wind direction (σ_θ) were recorded at 10-m height above the playa surface at the southern station. The time interval between passage of the same feature over these stations depended on wind direction, and decreased as the wind shifted toward the northeast. Two stations are in general sufficient only to generate an apparent velocity of translation. The apparent velocity obtained is 2.85 m/sec at 7:30 AM PST versus ~ 8.0 m/sec at 10 m recorded by cup anemometer. These experiments will be repeated in the future as part of validation exercises for atmospheric water vapor retrieval, but instead using a network of surface water vapor measurement stations. Such areal arrays of observations should define more precisely the geometry of water vapor movements and permit a better comparison with wind speed measurements obtained with meteorological instruments.

Method 2 - In the absence of the source and sink terms E − P (a good approximation for Mojave Desert conditions in late July), Equation 5 gives

$$\bar{U}_s = - \frac{\partial W/\partial t}{\partial W/\partial s} \qquad (6)$$

To estimate $\bar{U}_s$ by this method, we generated averages of W and $\partial W/\partial s$ for the area common to the four water vapor maps of Figure 3. The derivative $\partial W/\partial s$ was formed from $\sqrt{[(\partial W/\partial x)^2 + (\partial W/\partial y)^2]}$. For this calculation the x- and y-axes were along the vertical and horizontal boundaries of each panel. Small adjustments for differences in panel orientation were also applied. Average values for the time and space derivatives of the common area, namely $\overline{\partial W/\partial t}$, $\overline{\partial W/\partial x}$, $\overline{\partial W/\partial y}$, and $\overline{\partial W/\partial s}$, are given in Figure 7. The values of $\bar{U}_s$ obtained

by application of Equation 6 have been plotted on the profile of rawinsonde-determined wind speed given previously in Figure 4. In Figure 4 the average value of the horizontal wind speed was calculated from the vertical profile to an altitude of 20,000 feet (altitude below which 99% of the water vapor resides) using Simpson's rule.

(3) Water Budget Method with Long-Time Averages

Peixoto (1973, p. 14) pointed out that a long time- (and areal-) averaged water vapor storage term $\langle \partial W/\partial t \rangle$ in Equation 1 is in general very small compared with the other terms, and thus for long enough averaging periods (*e.g.*, seasonal or yearly) the water vapor flux divergence can be used to estimate $\langle \overline{E-P} \rangle$. We looked at the precipitable water measurements obtained from the Edwards AFB, California, rawinsonde observations covering the period of 1986-present to understand the gross properties of the (twice daily sampled) precipitable water time series at this locality. Figure 8 illustrates both the long- (seasonal) and short-term variation of precipitable water W(t). Figure 9 is the average value $\langle W(t_N) \rangle$ of the departure of W(t) from its mean value $\langle W \rangle$ over the time interval as calculated from the formula

$$\langle W(t_N) \rangle = \frac{1}{N\Delta t} \sum_{i=1}^{N} [W(t_i) - \langle W \rangle] \qquad (7)$$

where Δt is the time interval between observations t_i. The average value of the time derivative $\langle \partial W(t_N)/\partial t \rangle = \partial \langle W(t_N) \rangle / \partial t \approx [\langle W(t_N) \rangle - \langle W(t_{N-1}) \rangle]/\Delta t$. The requirement of long time averages may be overly restrictive. Thus from the record of Figure 9, time intervals of slowly changing $\langle W(t_N) \rangle$ can be identified. For example, the period of days 240 - 360 in 1986 is an interval where the derivative is small, while for the period of days 1 - 240, the derivative is comparatively large. The actual condition is that $\langle \partial W/\partial t \rangle \ll \langle \nabla \cdot \int \rho q dz \rangle$, and so a complete discussion requires evaluation of the flux divergence. The spatial derivative requires observations at multiple stations. The question of estimating the magnitude of this term from the single-station rawinsonde records using its time variability is under study.

Acknowledgments

We want to thank Ms. Marian Durran, 6521 RANS/TSRCP, Edwards AFB for supplying the rawinsonde data. Mr. Tony Garcia of Molycorp (Division of Unocal) kindly made available the meteorological data from their tower at Ivanpah Playa. Steve Adams of JPL provided much appreciated computational support. This paper presents the results of one phase of research carried out at Jet Propulsion Laboratory, California Institute of Technology, under a contract with the National Aeronautics and Space Administration.

References

Bruegge, C.J., J.E. Conel, J.S. Margolis, R.O. Green, G. Toon, V. Carrere, R.G. Holm, and G. Hoover, 1990, *SPIE Vol. 1298*, 150-163.

Brutsaert, W., 1979, *Boundary-Layer Meteorol.*, 16, 365-388.

Brutsaert, W. 1982, *Evaporation into the atmosphere*, D. Reidel Publishing Company, Boston, 299 pp.

Brutsaert, W., 1986, *American Geophysical Union Paper No. 5W0661*, 39S-45S.

Brutsaert, W., and J.A. Mawdsley, 1976, *Water Resour. Res.*, 12(5), 852-858.

Carrere, V., J.E. Conel, R.O. Green, C. Bruegge, J. Margolis, and R. Alley, 1990, Proceedings of the Second Airborne Visible/Infrared Imaging Spectrometer (AVIRIS) Workshop (R.O. Green, ed.), *JPL Publication 90-54*, Jet Propulsion Laboratory, Pasadena, California, 107-128.

Carrere, V., and J.E. Conel, 1991, Comparison of two techniques for recovery of atmospheric water vapor total column abundance from imaging spectrometer data: sensitivity analysis and application to Airborne Visible/Infrared Imaging Spectrometer (AVIRIS) data, to be published.

Carslaw, H.S., 1950, *An introduction to the theory of Fourier's series and integrals (Third edition)*, Dover Publications, Inc., New York.

Conel, J.E., R.O. Green, V. Carrere, J.S. Margolis, G. Vane, C. Bruegge, and R.E. Alley, 1989, *IGARSS '89 Symposium Proceedings*, Vol. 4, 2658-2663.

Conel, J.E., R.O. Green, V. Carrere, J.S. Margolis, R.E. Alley, G. Vane, C.J. Bruegge, and B. Gary, 1988, in Proceedings of the Airborne Visible/ Infrared Imaging Spectrometer (AVIRIS) Performance Evaluation Workshop (G. Vane, ed.), *JPL Publication 88-38*, Jet Propulsion Laboratory, Pasadena, California, 21-29.

Csanady, G.T., 1969, *J. Atmos. Sci.*, 26, 414-426.

Deardorff, J.W., 1968, *J. Geophys. Res.*, 73, 2549-2557.

Frouin, R., and E. Middleton, 1990, *Proceedings of AMS Symposium on FIFE*, 70th AMS Annual Meeting, Anaheim, California, 135-139.

Gao, B.C., and A.F.H. Goetz, 1990, *J. Geophys. Res.*, 95, 3549-3564.

Green, R.O., V. Carrere, and J.E. Conel, 1990, *Proceedings of Image Processing '89, American Society for Photogrammetry and Remote Sensing, Sparks, Nevada*, 31-44.

Green, R.O., 1991, Proceedings of the Third Airborne Visible/Infrared Imaging Spectrometer (AVIRIS) Workshop (R.O. Green, ed.), this publication.

Liu, W.T., K.B. Katsaros, and J.A. Businger, 1979, *J. Atmos. Sci.*, 36, 1722-1735.

Liu, W.T., 1986, *Mon. Wea. Rev.*, 114, 1591-1602.

Liu, W.T., 1990, *Surface waves and fluxes, Vol. II* (G.L. Geernaert and W.J. Plant, eds.), Kluwer Academic Publishers, The Netherlands, 293-309.

Peixoto, J.P., 1973, *WMO/IHD Report No. 20*, World Meteorological Organization, Geneva, 83 pp.

Peixoto, J.P. and A.H. Oort, 1983, in *Variations in the global water budget* (A. Street-Perrott, *et al.*, eds.), D. Reidel Publishing Co., Boston, 5-65.

Saffman, P.G., 1962, *Quart. J. Roy. Meteor. Soc.*, 88, 382-393.

Smith, F.B., 1965, *Quart. J. Roy. Meteor. Soc.*, 91, 318-329.

Taylor, A.D., 1982, *J. Atmos. Sci.*, 39, 837-850.

World Meteorological Organization, 1988, Concept of the global energy and water cycle experiment, *WMO/TD-No. 215 (World Climate Research Program - 5)*.

Zauderer, E., 1989, *Partial differential equations of applied mathematics*, John Wiley and Sons, New York, 891 pp.

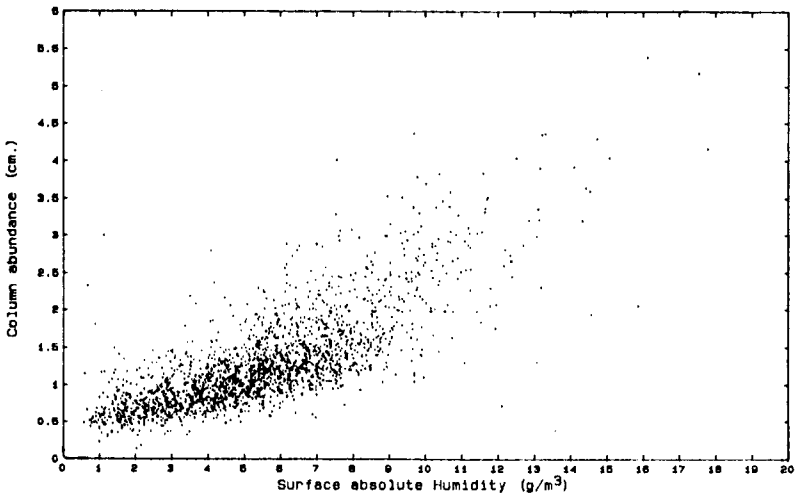

Fig. 1. Scatter plot of water vapor column abundance vs the surface value of absolute humidity for 2105 rawinsonde observations over the period 1986-present. Data courtesy of 6521 RANS/TSRCP, Edwards AFB.

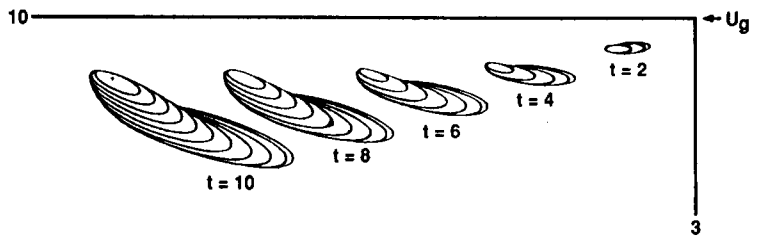

Fig. 2. Evolution in the Ekman layer of an instantaneous release at the surface. U_g is the geographic wind direction. The distance, height, and time coordinates are in non-dimensional units. From Taylor (1982).

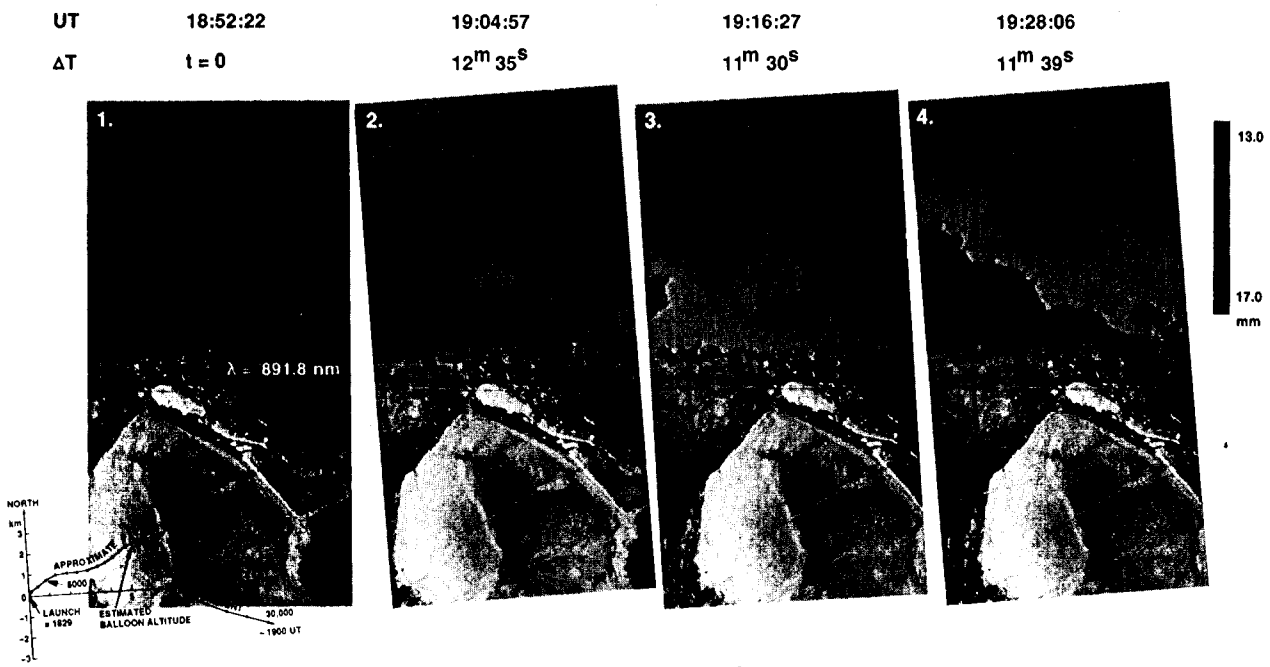

Fig. 3. Changes in water vapor column abundance with time at Rogers Dry Lake, July 23, 1990.

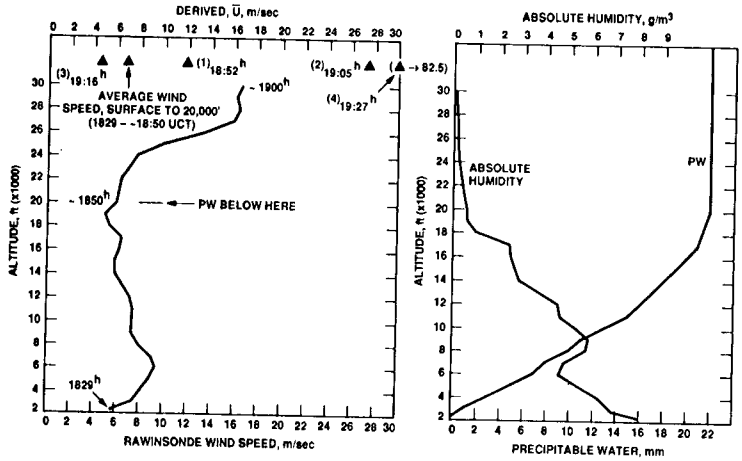

Fig. 4. Vertical profiles of wind speed, absolute humidity and precipitable water (PW) from the July 23, 1990 (18:29 hours UT) rawinsonde launch at Edwards AFB. The wind speeds Ū are derived from the image sequence of Figure 3 via Equation 6.

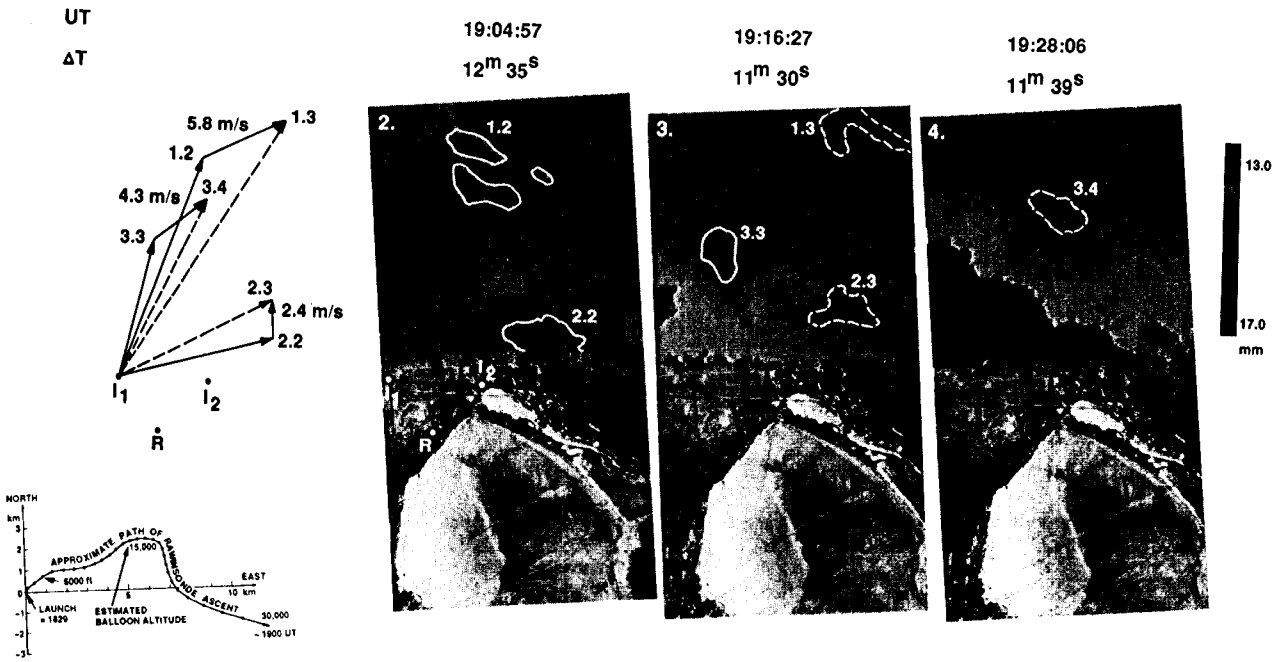

Fig. 5. Examples of possible displacements of water cloud features between water vapor scenes of Figure 3. The notation m.n = feature m.panel n.

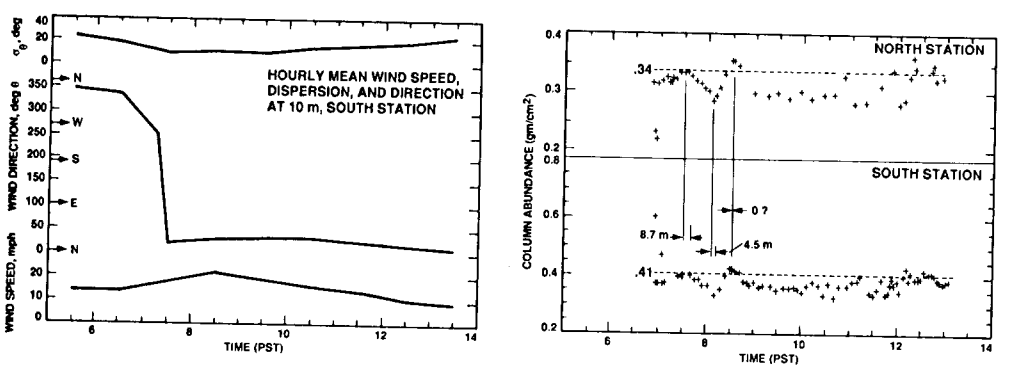

Fig. 6. Translation of water vapor features at Ivanpah Playa as measured with 940 nm water vapor channel of the Reagan sun photometers, March 7, 1991. Wind data courtesy of Molycorp, Division of Unocal.

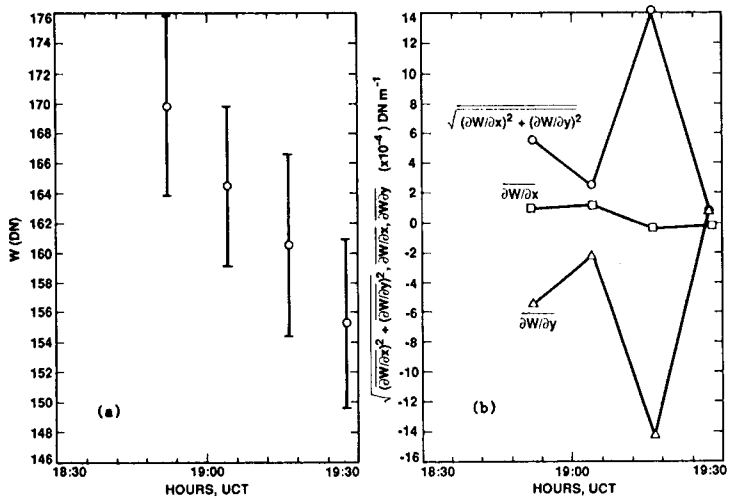

Fig. 7. (a) Time variability, and (b) Gradients of water vapor abundance averaged over the common area of successive water vapor maps in Figure 3.

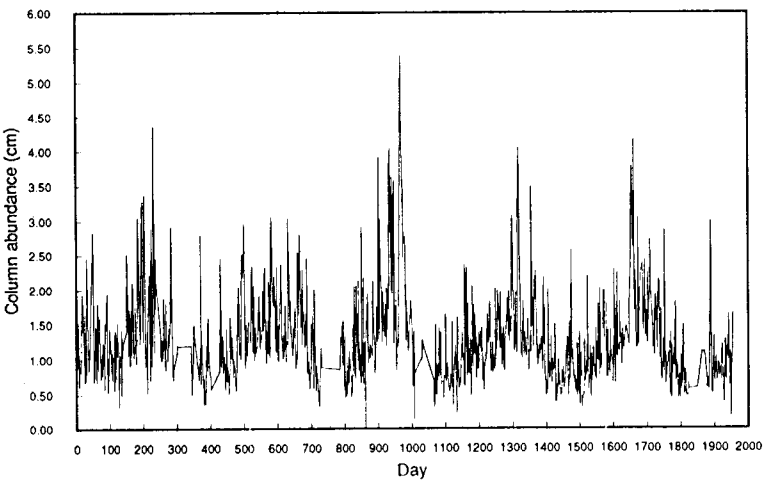

Fig. 8. Time series of water vapor column abundance as measured by rawinsonde for the period 1986-present, Edwards AFB, California. Data courtesy of 6521 RANS/TSRCP EAFB.

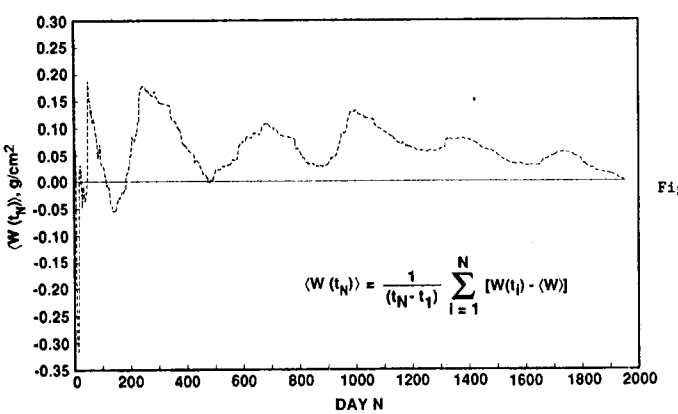

Fig. 9. Average value of the precipitable water abundance as function of time, derived from the time series of Figure 8.